A&A manuscript no.
(will be inserted by hand later)

Your thesaurus codes are:
07.03.1

ASTRONOMY AND ASTROPHYSICS

The effect of some solar wind disturbances on the plasma tail of a comet: Models and observations

Rudolf Wegmann

Max-Planck-Institut für Astrophysik
D-85748 Garching Germany
email:ruw@mpa-garching.mpg.de

Received November ,1999; accepted ,2000

Abstract. The effect of several solar wind disturbances on the plasma tail of a comet is studied by means of MHD model calculations. In particular, high speed streams (HSS) and non compressive density enhancements (NCDE) are investigated. Interplanetary shock waves, changes of the flow direction and current sheets are reconsidered. It is shown that HSSs, NCDEs and shocks can cause tail disconnections (DE). The DEs associated with these three solar wind disturbances can be distinguished by their morphology. These differences in appearance can be seen in observed DEs. For some DEs plausible solar wind triggers have been identified by observers. These corroborate the findings of the model calculations.

1. Introduction

The plasma tail of a comet is shaped by the solar wind. Therefore, it is sensitive to changes and disturbances in the solar wind. We could use the cometary tail as a measuring instrument (free of charge) if we were only able to understand what it is telling us. Magnetohydrodynamic (MHD) model calculations are an ideal means to study the response of the comet to well specified solar wind conditions. Such models are therefore a valuable tool to decipher the comet's message.

Most spectacular are tail disconnections events (DE). Although there is no consensus in the literature on the formal definition of a DE, the main feature is that "a major portion of the tail disconnects from the coma and falls away" (Farnham & Meech 1994, p.420). Several researchers have identified the DEs during comet Halley's 1986 apparition (Niedner 1986, Celnik & Schmidt-Kaler 1987, Delva et al. 1991, Yi et al. 1994, Voelzke & Matsuura 1998, and Brandt et al. 1999). Much effort has been spent to demonstrate that there is a close association between DEs and crossings of the heliospheric current sheet (HCS) (Niedner 1986, Yi et al. 1994, Voelzke & Matsuura 1998, and Brandt et al. 1999). It is now widely accepted that such an association exists, but it is less obvious that this correspondence is one-to-one.

Delva et al. (1991) correlate solar wind events in the VEGA data with events in comet Halley's tail. Their finding: "For the 22 DEs ... we find a possible correlation with SB [= sector boundaries] in four cases, a likely one in six cases and in two cases a SB as well as a high speed stream may be correlated with the DE. ... In the other 10 cases, a DE was observed although no SB was registered at the corresponding time. This indicates that a SB crossing is certainly not a necessary condition for the generation of a DE. On the other hand ... [SB crossing] is not a sufficient condition for DE. ... There is an indication that HSS also play a role." (Delva et al. 1991, p.707).

The model of Niedner and Brandt (1978) assumes that the magnetic field in the HCS reconnects when caught in the comet and so tears off the tail. Several efforts to corroborate this disconnection model by MHD model calculations failed (Fedder et al. 1984, Schmidt-Voigt 1989, Yi et al. 1996).

It has been shown in MHD model calculations (e.g. Schmidt & Wegmann 1982, Fedder et al. 1984) and confirmed by the ICE spacecraft at comet Giacobini-Zinner (see Slavin et al. 1986) that the cometary plasma is diamagnetic. The plasma tail is a narrow ribbon confined by two magnetic flux lobes. Therefore, the reconnected magnetic field could take only a small fraction of the tail with it.

It is discomforting, that the HCS sometimes seems to succeed in disconnecting the tail, but sometimes fails. The field reversal in the HCS is always present and should lead to field reconnection and tail disconnection. The statistical evidence seems to be more in favour of something which is more loosely coupled with the HCS. In view of this observational and theoretical evidence it may be worthwile to search for other mechanisms by which the HCS and its companions could trigger a DE.

In a previous paper (Wegmann 1995) we have demonstrated how an interplanetary shock wave can generate a DE. It is clear, however, that not all observed DEs can be caused by shocks, since comets are not hit by shocks frequently enough.

In view of the close association of the HCS with high speed streams, the statistical evidence could be also in favour of high speed streams as agent. Statistical analysis shows that the DE starts about .75 days (Niedner & Brandt 1978) or almost 1 day (Yi et al. 1994, Brandt et al. 1999) after the HCS has met the comet. At this time most of the HCS has passed the comet, and there is only little field left in the comet to reconnect. The time delay of the order of a day is an indication that the DE is caused by something which comes after the HCS. The HSS is the most likely candidate.

In this paper we investigate the effect of an HSS on the plasma tail. The result is a tail disconnection which is accompanied by a kink in the tail as it is frequently observed. We show that a simple rotation of the solar wind's flow direction produces a gradual turning of the tail, but no kink. Another test calculation demonstrates that the magnetic field enhancement in the HSS is important for the generation of a DE.

The HCS is often associated with a noncompressive density enhancement (NCDE) (Winterhalter et al. 1994). Motivated by this observational finding we investigate the effect of an NCDE on the plasma tail. It is shown that this also leads to a DE. This may explain the mechanism how the HCS itself can affect the tail.

The DEs generated by a shock, an HSS or an NCDE have different properties. These can be used to diagnose from an observed DE its most likely cause.

The plan of this paper is as follows: In section 2 we recall some basic facts of cometary MHD, in particular the scaling law for densities and column densities. In section 3 we investigate the effect of a high speed stream, in section 4 that of a change in solar wind flow direction. In section 5 we consider a HSS without magnetic field enhancement, and in section 6 a sudden transition from fast to slow wind. In section 7 we discuss the effect of a current sheet and in section 8 that of an NCDE. We recall our calculations for an interplanetary shock wave in section 9. Finally, we study in section 10 the effect of a full corotating interaction region. In section 11 we discuss some observations and their relation to our model calculations. In section 12 the results are compiled in a sort of 'dictionary' which allows to translate solar wind disturbances into tail events (and vice versa). The paper is summarized in the concluding section 13.

Several other solar wind discontinuities have already been treated. We mention in particular the rotation of the magnetic field orientation, which can generate tail rays (Schmidt & Wegmann 1982, Rauer et al. 1995, Wegmann et al. 1996). Other solar wind features, such as coronal mass ejections, will be studied in the future.

2. MHD models and scaling laws

The plasma flow in a comet can be described by the equations of ideal magnetohydrodynamics (MHD) with source terms (see e.g. Schmidt & Wegmann 1982, Wegmann 1995). One can combine the gas production rate G, the outflow velocity w from the nucleus, the mean mass m_C of a cometary particle, the ionisation rate σ and the solar wind mass flux $\rho_\odot u_\odot$ to an *interaction length scale*

$$R_I = \frac{\sigma m_C G}{4\pi w \rho_\odot u_\odot} \tag{1}$$

which determines the size of the region where the solar wind interacts with the comet.

We adopt a coordinate system $\mathbf{x} = (x, y, z)$ centered at the nucleus with x pointing towards the Sun. The y axis is so that the interplanetary magnetic field (IMF) is parallel to the xy-plane, which we call the IMF plane. The xz-plane is called the 'perpendicular plane'. Mass density ρ, number density n and velocity $\mathbf{u}$ are normalized by the corresponding solar wind quantities $\rho_\odot$ and $u_\odot$ to

$$\hat{\rho} = \frac{\rho}{\rho_\odot}, \qquad \hat{n} = \frac{m_C\, n}{\rho_\odot}, \qquad \hat{\mathbf{u}} = \frac{\mathbf{u}}{u_\odot}. \tag{2}$$

When the spatial coordinate $\mathbf{x} = (x, y, z)$ is measured in units of R_I, and time t is counted in units $R_I/u_\odot$ then under certain simplifying assumptions which are detailed in the paper by Wegmann et al. (1999), the equations governing the cometary plasma flow, rewritten in the normalized variables of (2), reduce to equations which do not contain any further parameters.

The main consequence of this is a *scaling law*: All physical quantities scale with the corresponding solar wind quantities, all lengths scale with the interaction scale length R_I, and time intervals scale with $R_I/u_\odot$. This scaling can be used to derive from observations information about the comet (in particular the production rate G) and the solar wind (Wegmann et al. 1999, 2000).

In this paper we are mainly interested in the brightness which is directly proportional to the column density n_{cd} of cometary ions. We recall (Wegmann 1995) that the density n_i and the column density n_{cd} of cometary ions scale like

$$n_i(\mathbf{x}) = \frac{\rho_\odot}{m_C} \cdot n_i^* \left(\frac{\mathbf{x}}{R_I}\right), \quad n_{cd}(\mathbf{x}) = \frac{\sigma G}{4\pi w u_\odot} \cdot n_{cd}^* \left(\frac{\mathbf{x}}{R_I}\right) \tag{3}$$

with functions n_i^* and n_{cd}^* which are independent of the solar wind and of the cometary parameters. It has been demonstrated by Wegmann et al. (1999) that along a line through the nucleus perpendicular to the sun-comet line,

$$n_i^*(0, \hat{y}, 0) \propto \hat{y}^{-2}, \qquad n_{cd}^*(0, \hat{y}) \propto \hat{y}^{-1} \tag{4}$$

with the nondimensional coordinate $\hat{y} = y/R_I$. This means that at a fixed point on this line the density as well as the brightness

$$n_i(0, y, 0) \propto \frac{1}{\rho_\odot u_\odot^2}, \qquad n_{cd}(0, y) \propto \frac{1}{\rho_\odot u_\odot^2}, \tag{5}$$

vary like the inverse of the dynamic pressure of the solar wind when all other parameters are kept fixed.

Table 1. Model parameters

variable	unit	slow1	fast1	big1	slow2	fast2
G	$10^{29}\mathrm{s}^{-1}$	2	2	10	1	1
n	cm^{-3}	20	10	7.5	5(15)	10.7
v_x	km/s	-359	-507	-401	-350	-391
v_y	km/s	-29(+38)	53	11	0	41
deflection	degrees	-4(+6)	6	1.6	0	6
B_x	nT	4.2	8.4(4.2)	4.2	3.45	7.6
B_y	nT	4.2	8.4(4.2)	4.2	3.45	7.6
T_p	10^5K	.5	3	.5	.5.	1.5
T_e	10^5K	1.4	2.2	1.4	0	0
p_p	10^{-10}dyn cm^{-2}	1.38	4.14	0.52	.345	2.18
p_e	10^{-10}dyn cm^{-2}	3.9	3	1.45	0.	0.
p_{mag}	10^{-10}dyn cm^{-2}	2.8	11.	2.8	.95	4.6
p_{dyn}	10^{-10}dyn cm^{-2}	430	430	200	100	280
R_I	1000 km	44.4	63.1	532	91.4	38.2
Ma		7.0	6.0	7.8	13.3	8.8
Ma$_A$		8.8	4.4	7.1	7.2	5.5

We have calculated models with parameters listed in Table 1. The parameters labeled 'slow1' and 'fast1' are for slow and fast solar wind data taken from Gosling et al. (1978), Fig. 2, eight hours before and after the interface of a corotating interaction region (CIR). The data 'big1' are for a big Halley type comet with solar wind data taken from Gosling et al. (1978), Fig. 1, two days before a CIR. The data 'slow2' and 'fast2' are for the oblique shock model (S4) calculated by Wegmann (1995). We calculate all models with photo-ionisation only, with a constant rate $\sigma = 10^{-6}$ s^{-1}, an outflow speed $w = 1$ km/s, and a mean mass $m_C = 20$ amu of a cometary molecule or atom. Only the shock model is calculated with the effect of charge exchange included (Wegmann 1995).

The small models $G = 1$ and $G = 2 \times 10^{29}$ s^{-1} are calculated on a grid which covers 300 000 km in front of the nucleus and to the sides, and 700 000 km along the tail. The big comet with $G = 10 \times 10^{29}$ s^{-1} is modeled on a grid five times as large.

We use the same numerical method as in our previous paper (Wegmann 1995). The code is based on a second order Godunov method using an approximate Riemann solver for the MHD equations. Spurious magnetic monopoles generated by numerical errors are removed in each time step (Schmidt-Voigt 1989). The code is able to capture shocks. The flow is calculated on a non equidistant grid with finest resolution of 8000 km near the nucleus for the small models. Advanced codes (e.g. Gombosi et al.1994) for the solar wind – comet interaction use also second order Godunov methods with an approximate Riemann solver. Adaptive grid refinement improves the accuracy of stationary models. These codes have not yet been used for time-dependent calculations.

3. High speed stream

In a high speed stream the velocity increases and the density decreases in such a way that the dynamic pressure $\rho_\odot u_\odot^2$ remains constant. This means that the solar wind mass flux $\rho_\odot u_\odot$ decreases, and R_I increases. When all other parameters remain constant, then it follows from equation (5) that neither n_i nor n_{cd} should be affected by a high speed stream. But in a HSS the magnetic field is enhanced by a factor of two (see e.g. Gosling et al. 1978, Fig. 3). The enhanced magnetic field transfers more momentum from the ambient solar wind to the central parts of the tail. Thus, the plasma moves faster, it becomes more tenuous. This is the main effect, which dims the comet when it enters an HSS, and which causes the comet to shed off part of its tail.

We started a time dependent calculation from the stationary model 'slow1' (see table 1). At time t=0 a high speed stream with parameters 'fast1' (see table 1) first hits the inflow boundary. The solar wind parameters change discontinuously. The discontinuity surface is inclined to the flow direction by 45 °. It is parallel to the interplanetary magnetic field (IMF).

The solar wind discontinuity is not in equilibrium. It resolves according to the Riemann problem into several waves. Since the magnetic field is parallel to the plane of the discontinuity there are only three waves, namely two shocks moving with the fast magnetosonic speed and a contact discontinuity moving with the flow speed. The slow magnetosonic speed and the Alfven speed are both zero since the field is transversal to the direction of wave propagation. Since the magnetic field is small, the resolution of the flow discontinuity can be calculated hydrodynamically. The result, shown in Figure 1 and in table 2, can be discribed as follows:

The component u_n of the velocity normal to the discontinuity surface increases in two steps. The fast flow

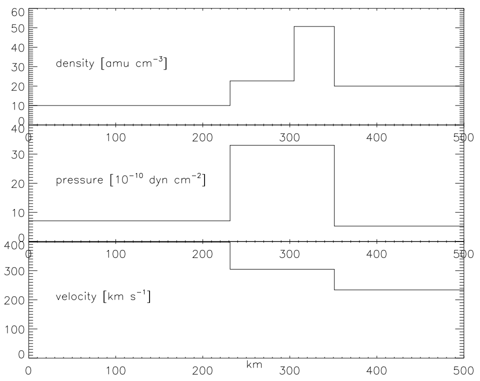

Fig. 1. Resolution of the discontinuous transition from 'slow1' to 'fast1' flow. Density, pressure and velocity profiles after 1 s.

Table 2. Resolution of the discontinuous transition from slow1 to fast1 wind

	fast1			slow1
ρ [amu cm^{-3}]	10.	22.6	50.7	20
p [10^{-10}dyn cm^{-2}]	7.1	33	33	5.3
u_n [km/s]	398	305	305	234

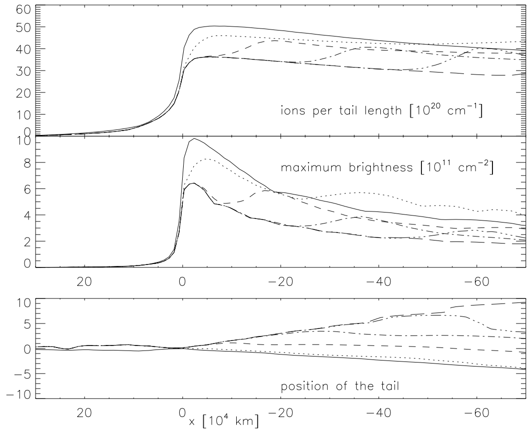

Fig. 3. The position of the tail (lower panel) the maximum brightness (middle panel) and the ions per tail length (upper panel) after 0 (solid), 1 (dotted), 2 (dashed), 3 (dash-dotted), 4 (dash-dot-dot-dot) and 5 hours (long dashes).

pushes from behind onto the slow flow. In the interaction region a density and a pressure hump develop, and the dynamic pressure increases by a factor of 3.3. This interaction region runs through the comet with a velocity of 350 to 470 km/s. It passes the ambient plasma in the computational grid in 30 to 45 minutes.

The central part of the tail reacts much more slowly. Figure 2 shows the brightness (proportional to the column densities) in the model calculation 0, 1, 2, 3, 4, and 5 hours after the HSS has entered at the lower left corner. The view is perpendicular to the IMF.

The tail is shaped by several effects.

First, the tail turns and so adjusts to the new flow direction of the solar wind. This becomes clearer in the lower panel of Figure 3 where the position of the tail is plotted at the same instances. (The tail position is defined as the point of maximal brightness in a cross-section perpendicular to the tail.) The tail is first shifted as a whole. But after three hours a kink develops at a distance of 350 000 km behind the nucleus. This kink becomes more pronounced after 4 hours.

Secondly, part of the tail recedes and the new tail adapts to the lower brightness pertinent to the new solar wind conditions. This can be seen most clearly in the middle panel of Figure 3 where the maximum brightness in sections across the tail is shown. In the first hour, a compressional wave runs through the tail which enhances the density and the maximum brightness all over the tail. But in the next few hours a clear second maximum in the tail develops. A 'cloud' is formed. This cloud moves downward. The tail settles down in a new steady state corresponding to the 'fast1' solar wind condition.

The cloud's motion is accelerated with an acceleration a=5.3 m s^{-2}. For comparison: the velocity along the tail axis can be approximated by an accelerated flow with a = 3.5 for 'slow1', and a = 9 m s^{-2} for 'fast1'. Hence, the acceleration of the cloud is between these two values.

The upper panel of Figure 3 shows the ions per tail length, i.e., the ions in Figure 2 integrated over the y-coordinate perpendicular to the tail axis. The curves start for t=0 from a high level. But after 2 hours they consist of a low and a high part, with the transition moving downstream as time proceeds. This shows clearly that the bright tail is disconnected, moves downstream and gives way to a dimmer tail.

A closer analysis shows that part of the tail's mass is severed from the coma and moves downstream. The solar wind has changed its direction. It blows now more from the side. The old tail has a luff and a lee side. This becomes most pronounced at that part of the tail where the severed dense cloud passes by. The massive cloud resists with some success the forces of the wind. On the lee of this cloud the tail is rarified.

The magnetic field is shown in Figure 4. The field is removed and cannot be replenished by the blocked solar wind (see the 'magnetic hole' in the far tail after 3 and 4 hs in Fig.4). The cloud itself is compressed by the action of the cross streaming solar wind. At the luff the magnetic field piles up (see the difference between the lower and the upper part of the tail in Fig.4 after 2, 3 and 4 hs). There is an enhancement of the total pressure in the cloud indicating an adiabatic compression. This confines the cloud and shapes it to the bright bar which connects the two parts of the tail pointing into the new and old flow directions.

Thus, the signature of the action of an HSS is a kink in the tail, formed by a bar connecting two tail segments pointing into different directions. At the inner end of the kink the tail seems to break off.

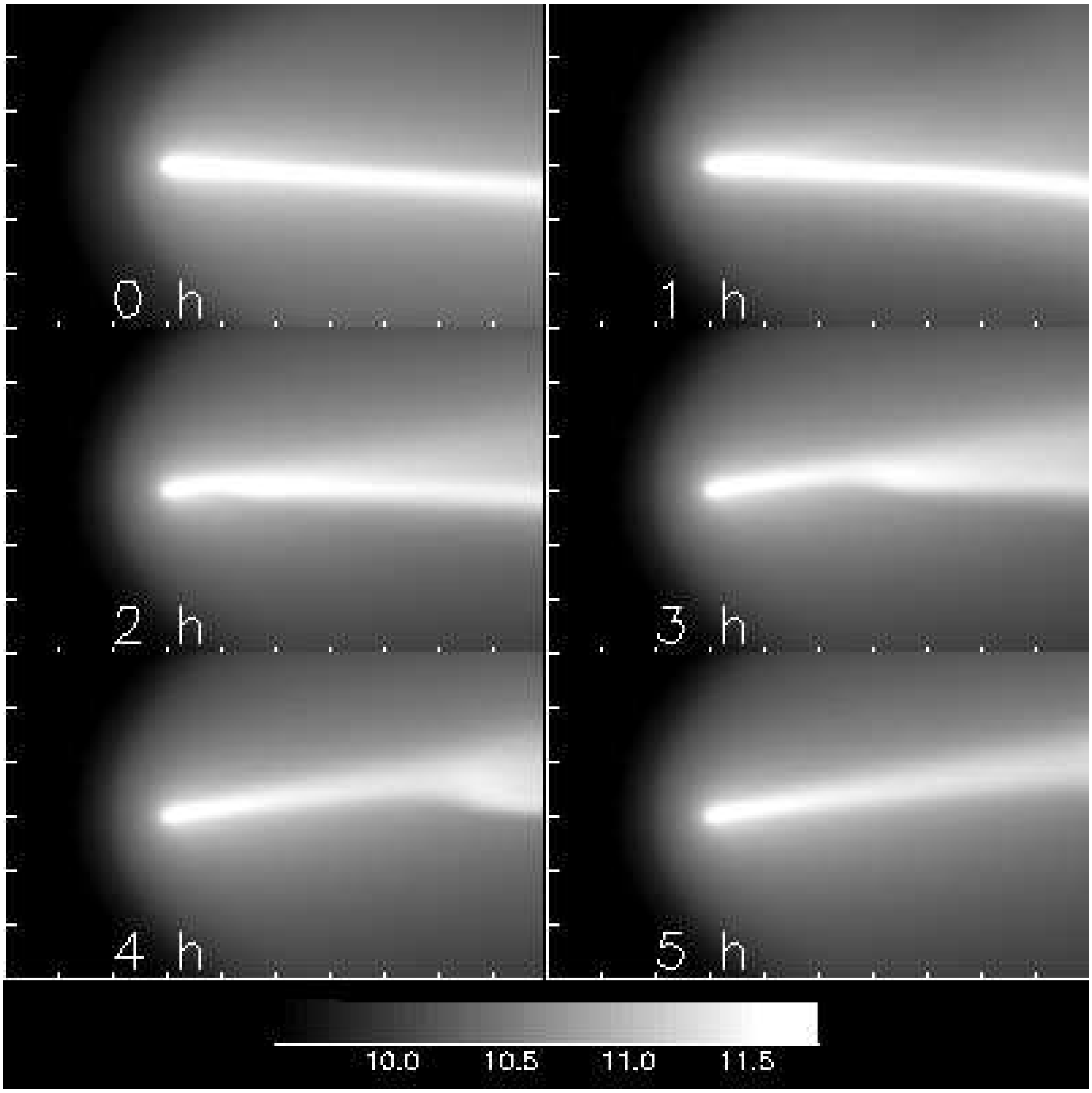

Fig. 2. Logarithms of the column densities [cm^{-2}] in a projection onto the IMF plane 0, 1, 2, 3, 4, 5 hours after the HSS entered at the lower left corner. The length scale is 100 000 km.

The kink is observable only when the line of sight forms an angle with the transverse component of the IMF. Figure 5 shows how the tail would look like for an observer in the plane of the IMF. After three hours a cloud appears in the tail. This cloud marks the position of the kink seen in Figure 2.

As we have argued before, the reduced brightness cannot be attributed to the changes in velocity and density alone, since the dynamic pressure remains unchanged. The effect is to a large extent generated by the enhanced magnetic field, which transfers much more momentum from the bystreaming solar wind into the tail and so accelerates the plasma more efficiently and in this way removes it from the tail which becomes more tenuous. To demonstrate this more convincingly we have repeated the calculation with the same parameters but with unchanged magnetic field. These calculations are shown in section 5.

But the tail morphology also cannot be generated by a simple change of the flow direction. This will be demonstrated in section 4.

4. Rotation of the velocity vector

Jockers and Lüst (1973, p.120) interprete two kink events at comet Bennett on April 2 and April 6, 1970 “as being

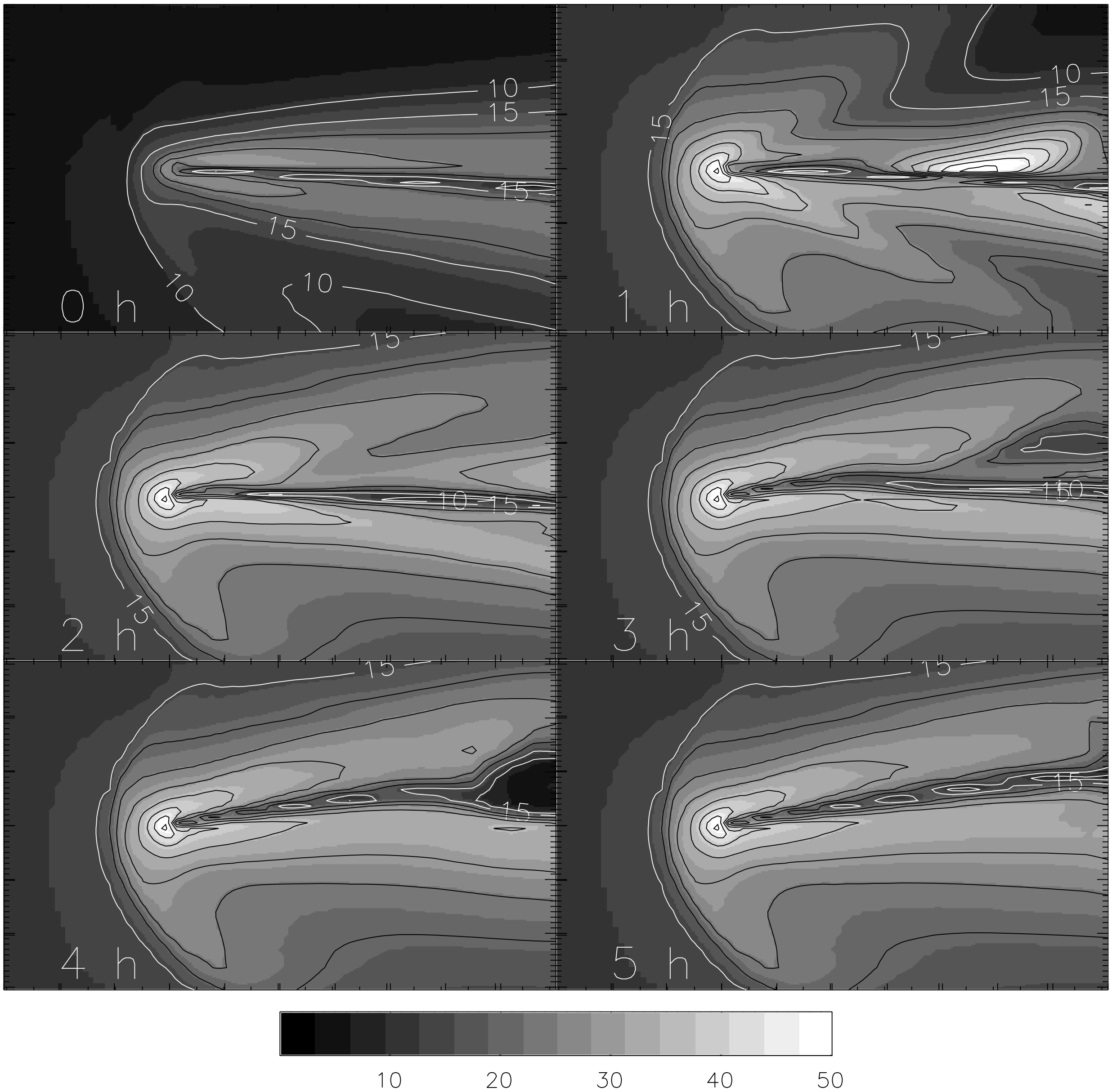

Fig. 4. The magnetic field strength [nT] in the IMF plane. The contour levels are 10(5)50 nT.

caused primarily by a change in the solar wind direction". In this section we single out the effect of a change in the flow direction and show that this is not quite sufficient to knock a kink into the tail.

The time dependent calculation is started from model 'slow1'. At time t=0 the solar wind velocity vector is rotated by 10° to the values of 'slow1' in brackets. A similar calculation has been done by Rauer et al. (1995) for different physical parameters and with a different numerical code but with basically the same result.

The result of our calculation is shown in Fig. 6. The velocity discontinuity is not quite in equilibrium. On one side (the lower side in Fig. 6) fast flow tries to overtake slow flow. This generates a compression which runs through the tail. On the opposite side the slow flow lags behind and gives way to a rarefaction wave. These discontinuities pass the ambient plasma in little more than half an hour. The main tail is compressed from one side. This enhances the brightness in the first two hours (see middle panel of Fig. 7).

After three hours the brightness decreases to new lower values. This dimming is due to the fact, that the new flow direction forms an angle of 51° with the magnetic field, larger than the old angle of 41°. The magnetic field relaxes its pressure from the lower side, the tail expands, becomes more diffuse and so reduces the maximum brightness.

The upper panel of Fig. 7 shows that the ion content remains nearly unchanged. There is no disconnection in this case. The lower panel of Fig.7 shows that the tail is shifted gradually to the new position. This is a consequence of the

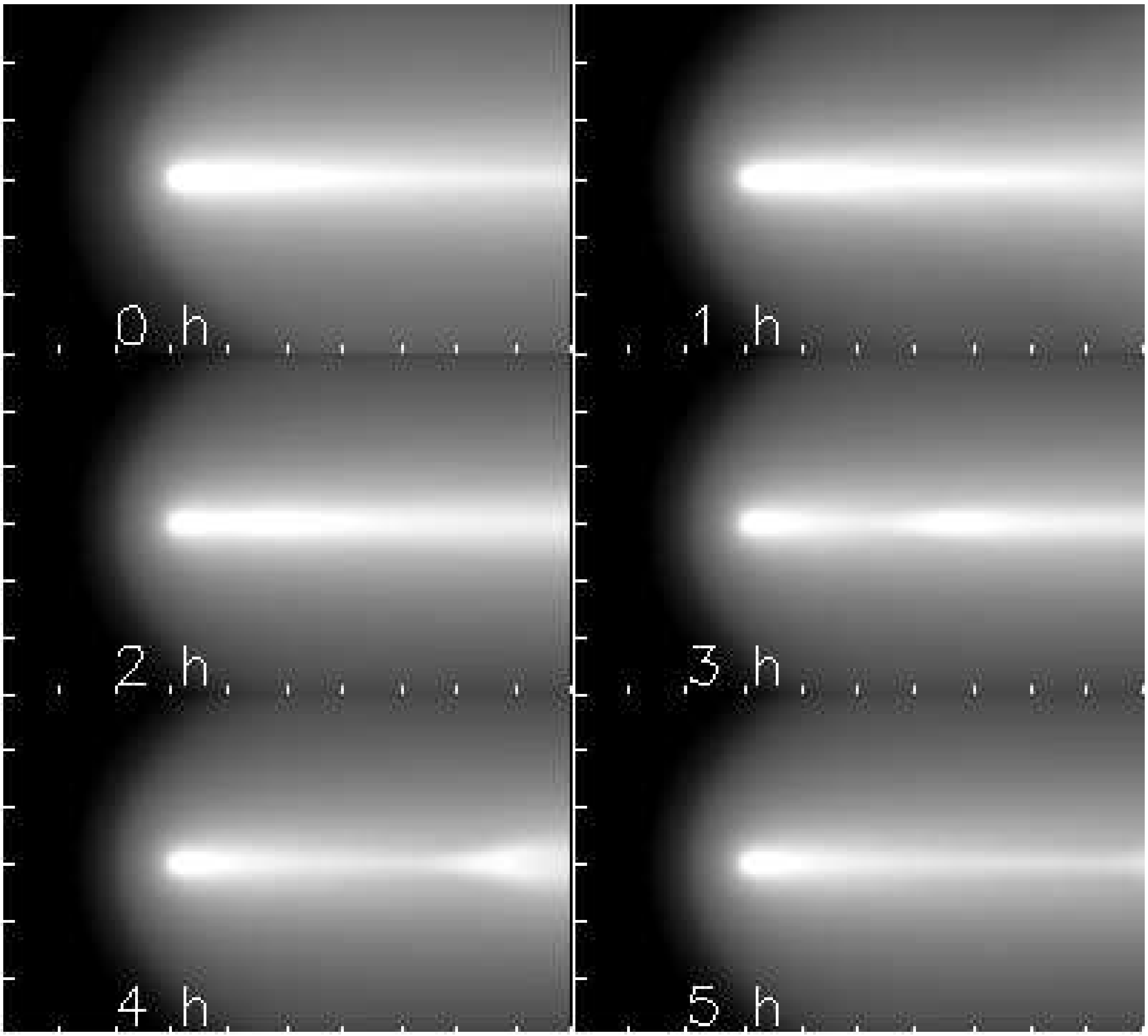

Fig. 5. The same as Figure 2 but in a projection onto the perpendicular plane.

fact, that the outer parts of the tail turn faster than the central part. The tail becomes, while turning, more diffuse. This is seen in Figure 6 where after three hours a spray develops on the lee side of the unrotated parts of the tail. There is no indication of a kink.

5. Effect of the magnetic field

We have seen in section 3 that an HSS should have little effect on the brightness of the plasma tail unless it is accompanied by an enhancement of the magnetic field. The argument was based on the scaling law which neglects the influence of the magnetic field. We test it by a numerical model calculation.

This calculation is also started from model 'slow1'. At t=0 the solar wind condition was changed to 'fast1' while keeping the magnetic field constant (the values of 'fast1' in brackets).

Figures 8 and 9 show that the situation resembles more the case of a simple direction change, treated in section 4, than the situation of a full HSS as described in section 3. The most striking difference to the HSS model is the lack of a clear second brightness maximum in the tail (see the middle panel of Fig.9). Therefore, one cannot identify a tail disconnection or even a cloud. The ions per tail length (upper panel of Fig.9) vary only very little with time. After 4 hours there is also a kink in the tail, but it is less pronounced than the kink in the corresponding Fig. 2.

6. From fast to slow wind

The transition from fast to slow wind is in general gradual. A sudden decrease in velocity is rarely observed. Nevertheless, it is interesting to model the reaction of the cometary tail to such an event.

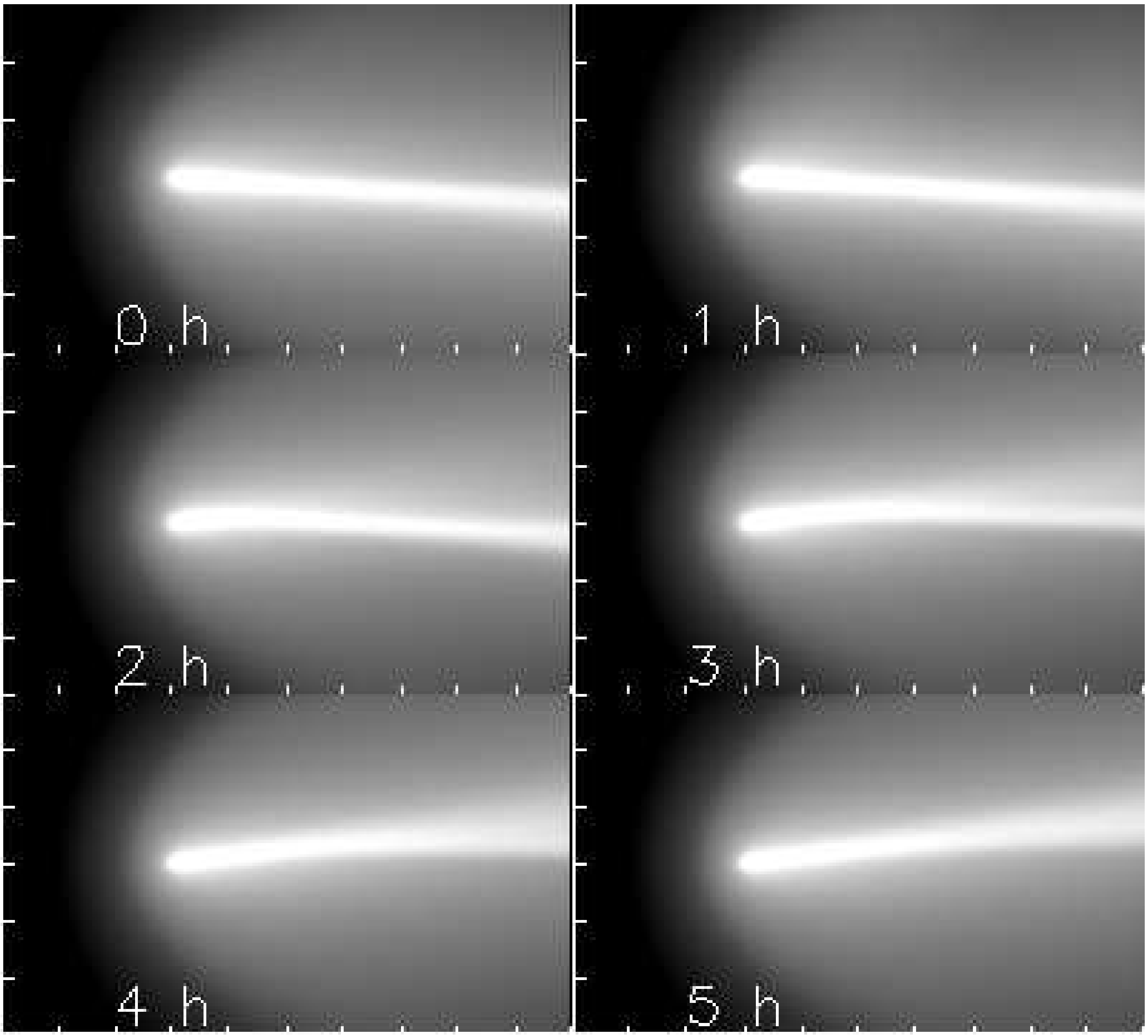

Fig. 6. The same as Figure 2 for a change in flow direction.

We start from the model 'fast1' and switch at time t=0 the solar wind conditions to 'slow1'. The discontinuity is not in equilibrium. It is resolved into several waves according to the Riemann problem. Since the magnetic field is transversal, there are only three waves namely two rarefaction waves moving approximately with the fast magnetosonic speed and a contact discontinuity moving with the flow speed. When calculated hydrodynamically the fast and the slow flow are connected by two intermediate states which are listed in table 3. The state after 1 second is shown in Fig. 10. The rarefaction fans are approximated by inverse shocks.

Fig. 11 shows that the tail is rotated by 10° and becomes brighter. The outer parts of the tail attain the new position faster than the central parts. In addition they brighten faster. This can be seen in the ion density distribution in a plane cut 600 000 km behind the nucleus (Fig. 13).

Table 3. Resolution of the discontinuous transition from fast1 to slow1 wind

	slow1			fast1
ρ [amu cm^{-3}]	20	6.6	3.1	10
p [10^{-10}dyn cm^{-2}]	5.3	.48	.48	7.1
u_n [km/s]	234	293	293	398

The originally kidney shaped contour lines are deformed after two hours to hearts. Only gradually they attain their final kidney shapes at the shifted position.

In view of this morphology, after three hours, the new tail, although only partly established, competes in brightness with the old tail. The tail splits into two well defined separated branches. The position of the tail shown in the lower panel of Fig. 12 after 3 hours is the position of the

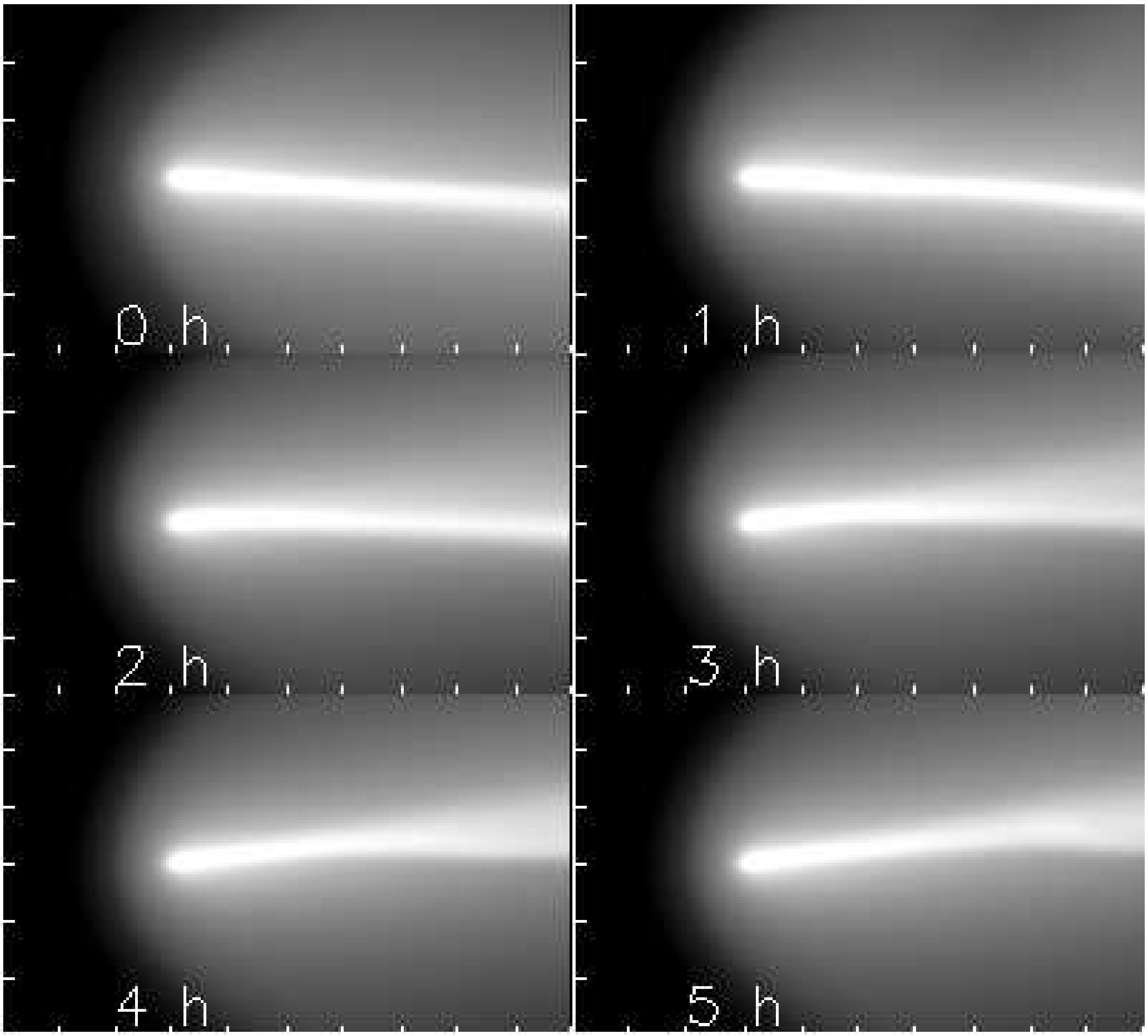

Fig. 8. The same as Figure 2 for an HSS without field enhancement

upper branch, which is distinguished as a clear maximum in brightness in cuts across the tail.

The branchpoint is not at the nucleus as one would expect for tail rays. The tail branches at a distance of about 200 000 km behind the nucleus. The tail is still split into two branches at later times. The branchpoint moves farther downstream and arrives after 5 hours real time at a distance of 400 000 km (see Fig. 11). Note that there is no condensation at the branchpoint! This is different from the morphology induced by a density enhancement (see section 8).

7. A current sheet

The heliospheric current sheet is considered by many as the most likely cause for most if not all DEs. In fact one can find in the literature statements as strong as: "[Analysis of] 19 DEs in Halley's comet leaves little doubt that DEs are associated primarily with crossings of the HCS and apparently not with any other properties of the solar wind such as high speed streams, dense regions, or dynamic pressure increases" (Brandt et al. 1999, p.76). Such a statement relies explicitly on the assumption that all (or most) DEs have a common cause. It relies implicitly on the assumption that DEs form a homogeneous class of phenomena.

In previous model calculations a density enhancement along the current sheet has been found but no tail disconnection (Fedder et al. 1984, Schmidt-Voigt 1989).

We start our calculation from model 'slow1' (in fact we start from the final state of the fast to slow transition reported in section 6). At time t=0 the IMF in the solar wind is replaced by its negative value.

There is numerical diffusion in the numerical code due to limited resolution of the computational grid. Thus, mag-

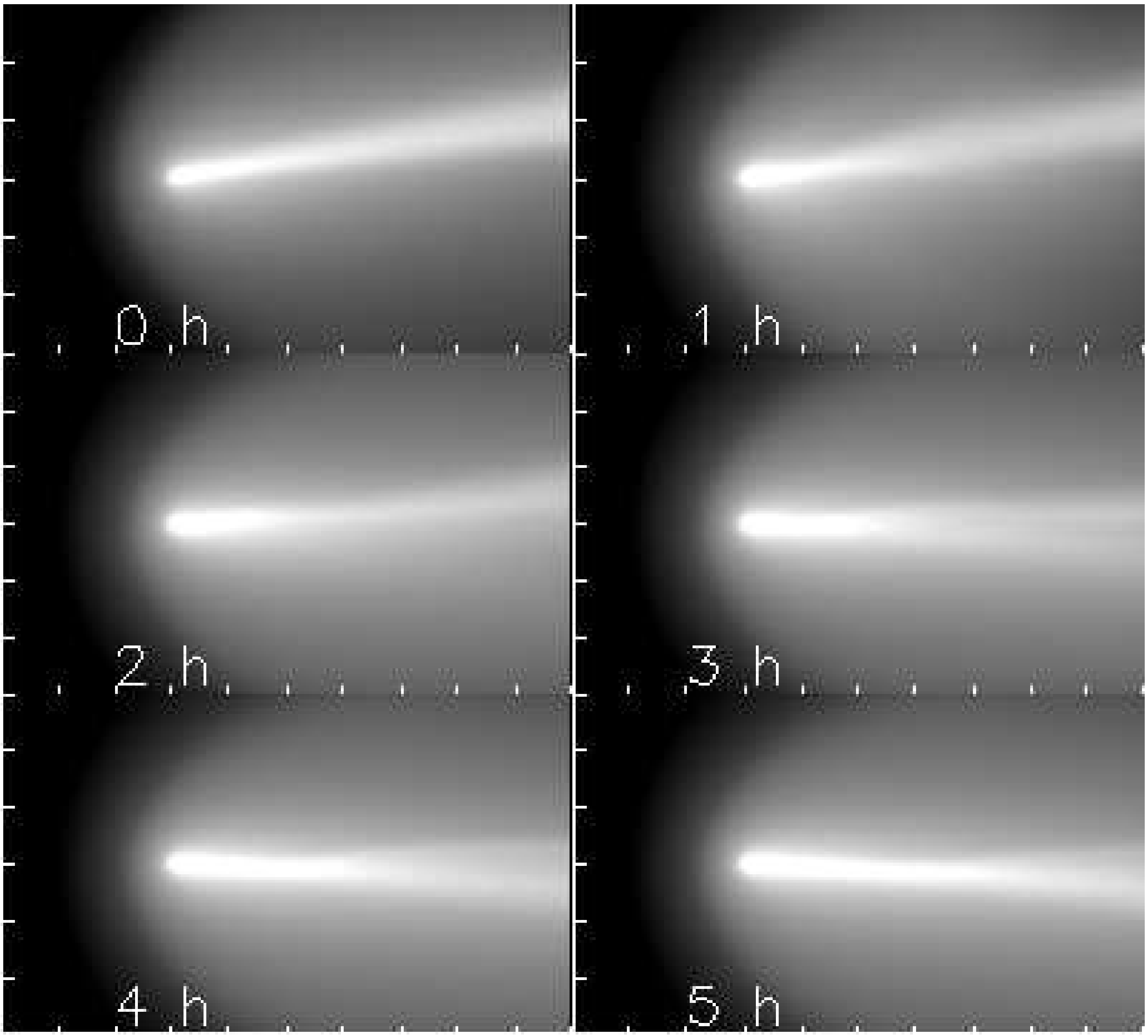

Fig. 11. The same as Figure 2 for a discontinuous change from fast to slow wind.

netic field of opposite polarity diffuses and cancels. Energy conservation transforms magnetic into thermal energy and so replaces magnetic by thermal pressure. Magnetic pressure acts with an adiabatic index $\gamma = 2$, while thermal pressure acts only with $\gamma = 5/3$. Thus by converting magnetic into thermal energy the plasma becomes more compressible. This has the consequence that the plasma near the current sheet is adiabatically compressed. The density is enhanced.

Figure 15 shows that there is no deflection of the tail.

The point of maximum brightness is in the stationary model 'slow1' at a distance of 20 000 km behind the nucleus. After 1 h it moves closer to the nucleus to a distance of 10 000 km and then recedes in an accelerated motion into the tail with an acceleration of 3.3 m s^{-2}. We recall from section 3 that this is only slightly below the acceleration in the stationary model 'slow1'. Therefore, the cloud is simply convected by the flow.

This blob in the tail is brighter than the coma for three hours. Due to the diffusion (or reconnection) the field around the HCS is depleted. Therefore, less momentum is transported to the central part of the tail where the flow remains slower and denser. This leaves its signature in the ions per tail length profile in the upper panel of Figure 15. After the passage of the current sheet the tail returns to its original appearance, which is insensitive to the sign of the magnetic field.

The blob in the tail can also easily be followed in the images shown in Figure 14. It is most conspicuous after 4 and 5 hours when the tail looks like a snake after swallowing a rabbit.

When the field is rotated by an angle α less than 180° then diffusion and reconnection can also deplete magnetic field but only the antiparallel component which is a fraction of $\sin^2(\alpha/2)$. In the case of a 90° rotation this amounts to 50%. The cloud in the tail found by Schmidt-Voigt

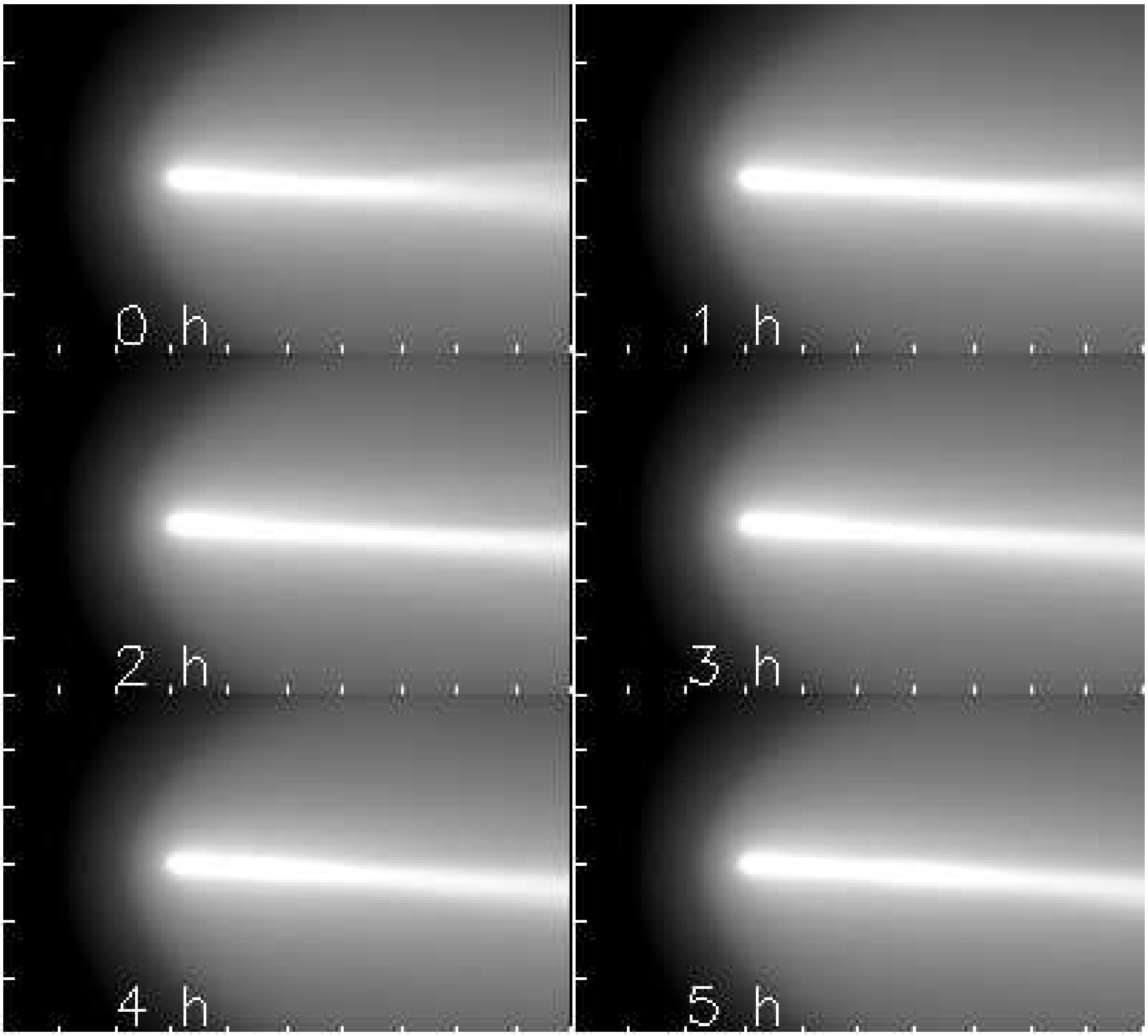

Fig. 14. The same as Figure 2 for the transition of a current sheet

(1989), p.444, in a simulation of a 90° field rotation can be explained by the same mechanism as described above in connection with our results for the current sheet.

The results of this section rely on the diffusion of magnetic field. The simulations simply use the diffusion caused by the numerical scheme. But as already noted by Schmidt-Voigt (1989) the numerical diffusion exaggerates the field diffusion in a cometary plasma by several orders of magnitude. Thus, the results of this section are not very realistic.

8. Non compressive density enhancement

High densities are sometimes observed when bulk speed is nearly constant and slow (less than 450 km/s). Since these density enhancements are not the result of a compression by stream interaction they are called *non compressive density enhancements* (NCDE) (Gosling et al. 1977). The magnetic field is not enhanced, proton and electron temperatures are low and vary in opposition to the density. Approximately one third of these events contain IMF reversals which are apparently not sector boundaries. The NCDEs occur typically as precursors of HSS (Gosling et al. 1977, p.5005). The average occurence of NCDEs is 2.7 events per month. NCDEs are apparently non recurrent, but primarily transient in nature. NCDE often appear to be discrete with recognizable beginnings and ends (Gosling et al. 1977,p. 5008).

The heliospheric current sheet is embedded in a plasma sheet (HPS) with a typical thickness of 320 000 km (Winterhalter et al. 1994). This HPS is characterized by high density. These high density peaks are of coronal origin. The coronal streamers (often of helmet-like appearance) are on eclipse photographs brighter than the background corona (Gosling et al. 1981, p. 5444). Superposed epoch plots of the solar wind proton density for 23 sector bound-

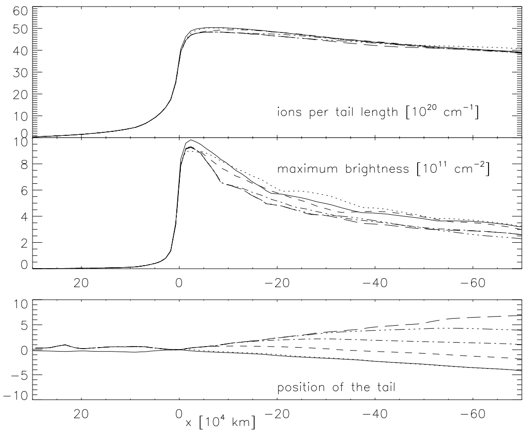

Fig. 7. The same as Figure 3 for a change in flow direction.

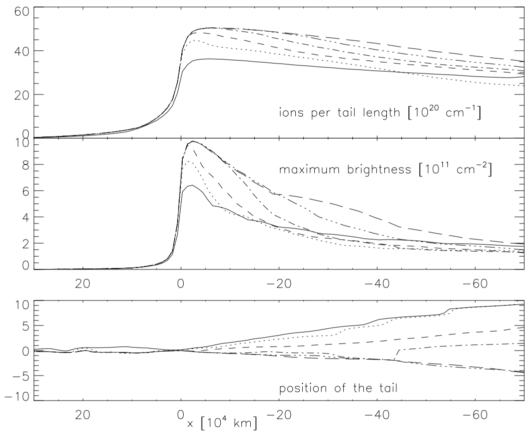

Fig. 12. The same as Figure 3 for a discontinuous change from fast to slow wind.

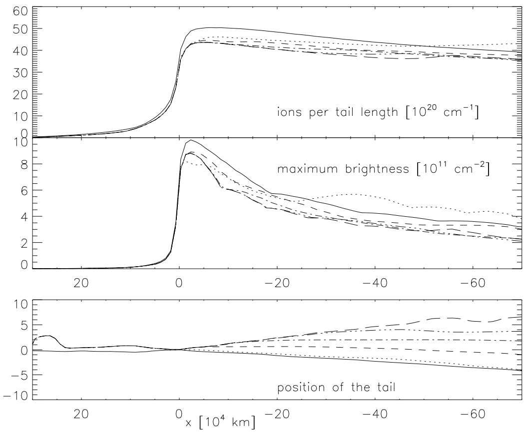

Fig. 9. The same as Figure 3 for an HSS without field enhancement

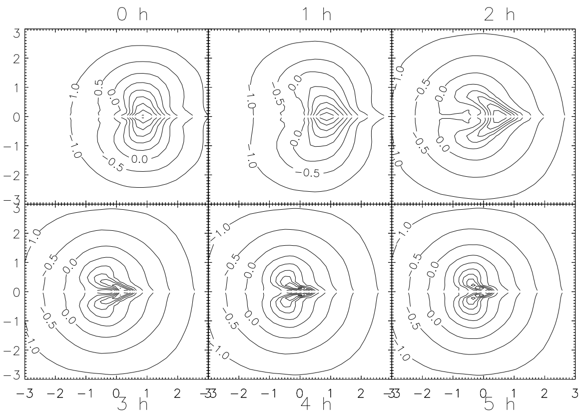

Fig. 13. Density n_i of ions in a plane cut through the tail 600 000 km behind the nucleus after 0, 1, 2, 3, 4, and 5 hours. The levels are - 1 (.5)3 for $\log(n_i)$. The size of each plot is 600 000 km squared.

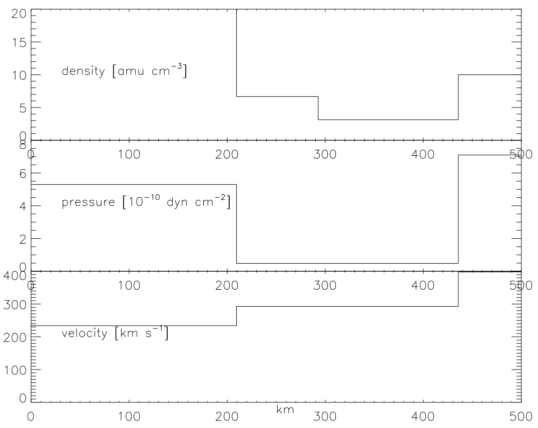

Fig. 10. Resolution of the discontinuous transition from 'fast1' to 'slow1' flow. Density, pressure and velocity profiles after 1 s.

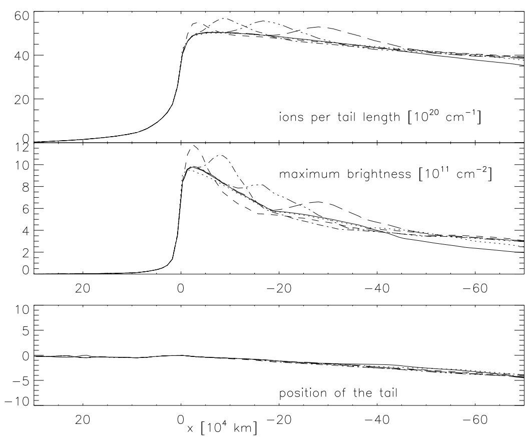

Fig. 15. The same as Figure 3 for the transition of a current sheet.

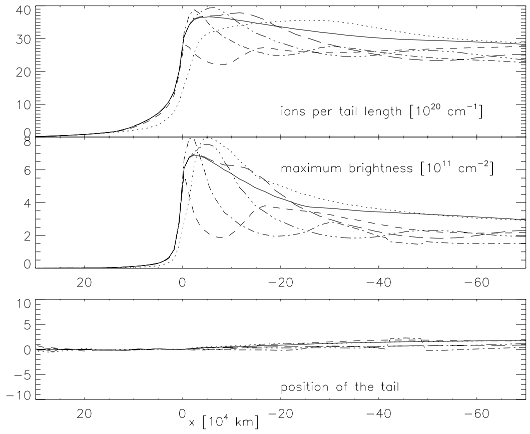

Fig. 17. The same as Figure 3 for a noncompressive density enhancement of 1h duration.

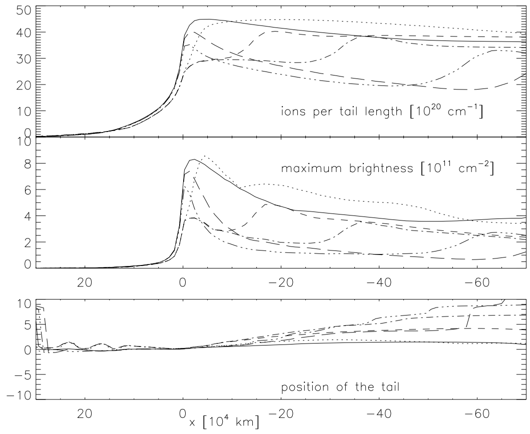

Fig. 20. The same as Figure 3 for an interplanetary shock.

aries show a distinct density peak at the position of the sector boundary which is well ahead and well separated from the density peak of the following stream interaction (Gosling et al. 1981, Fig.1).

For modeling an NCDE we start from model 'slow2', enhance at time t=0 the solar wind density by a factor of three from 5 to 15 amu cm^{-3} (the values of 'slow2' in brackets), and switch back to the original density after 1 hour.

In an NCDE only the density $\rho_\odot$ increases with all other quantities unchanged. This implies that R_I decreases, and the dynamic pressure increases. It follows from equation (5) that density n_i and column density n_{cd} both decrease proportional to $\rho_\odot^{-1}$. This means that the brightness would finally be reduced by a factor of three if the high density solar wind would persist.

We see in Fig. 17 that in the first hour the tail is compressed and attains higher maximal brightness, while at the same time the ions are moved from the coma into the tail. The point of maximum brightness starts to move into the tail after 40 minutes. This brightness peak is accelerated. After 80 minutes, shortly after the solar wind has returned to its original state, the density in the coma recovers and develops a new brightness peak. But a gap between the renewed coma and the receding old tail opens and widens. After 3 hours the brightness maximum in the tail is no longer accelerated but continues to move with a constant speed of about 75 km/s.

Fig. 16 shows that after 3 hours downstream of this cloud the tail fans out. This is due to the fact that the low total pressure in the sheet corresponding to the high density solar wind allows the tail to expand laterally. The new tail first appears as a crescent near the nucleus. The outer parts of this crescent move fast and close up to the old receding tail. The merging tails contribute to the fan like appearance of the far tail.

In the IMF plane the tail is still well confined by the magnetic field. The tail can expand more easily perpendicular to the field. Therefore, the lateral expansion of the tail is much more pronounced in a projection onto the perpendicular xz-plane (see Fig. 18).

9. Shock

For comparison we recall the results of the action of an interplanetary shock on the cometary tail calculated by Wegmann (1995). The calculation started from model 'slow2'. At t=0 the solar wind conditions were changed to 'fast2'. This corresponds to a shock wave of Mach 2 which propagates with a speed of 357 km/s relative to the upstream flow 'fast2'. After three hours the solar wind conditions were changed back to its original values 'slow2'. In this calculation charge exchange ionisation was included. This has little influence on the overall phenomenology.

The middle panel of Fig. 20 shows that after the initial compression of the tail, which leads to enhanced brightness after 1h, the brightness of the coma drops by about a factor of 2 while the brightness of the far tail remains nearly unchanged. The dimming of the coma is quite in accordance with the increase in dynamic pressure in the shock. The disconnected tail moves downstream with an acceleration of a=6.5 m s^{-2}.

The upper panel of Figure 20 shows that also the ion content per unit tail length is decreased by a factor of 1.5. This means that the tail is really pushed away by the shock. The shock wave is more efficient than the high speed stream (cf. Fig. 3). The turn of the tail in the shock is more gradually. There is no kink visible in the bottom panel of Fig. 20. This feature distinguishes the shock induced DE from that caused by an HSS.

Figure 19 shows that the new tail, formed after the inverse shock, points into the original direction while the disconnected tail recedes along the direction of the shocked flow. This leads finally to a constellation where the tail looks 'diagonally split' as observed e.g. at comet Borelly on 24 July 1903 (see Brandt 1982, Fig. 9).

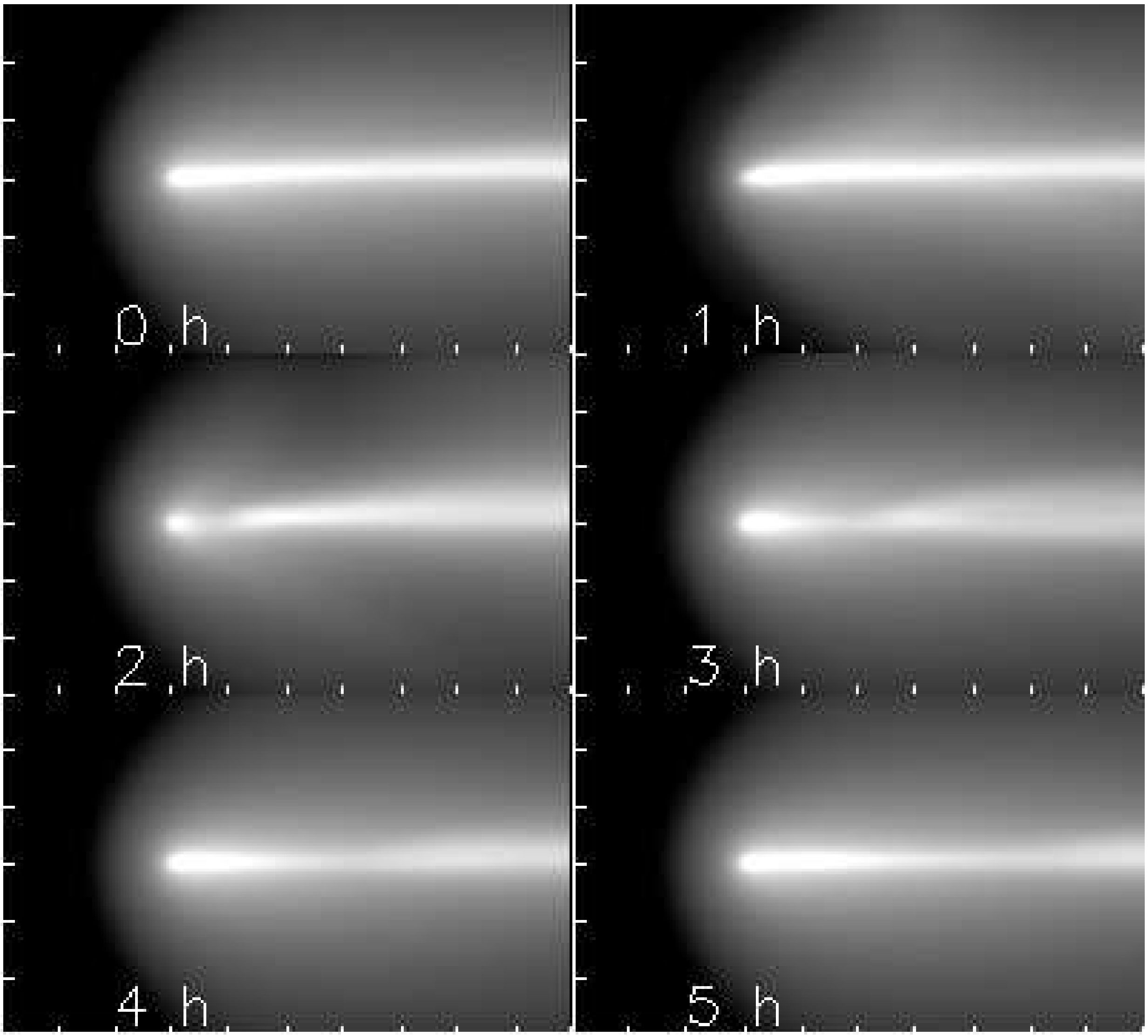

Fig. 16. The same as Figure 2 for a noncompressive density enhancement of 1h duration.

Fig. 21 shows the tail projected onto the perpendicular xz-plane. After 3 hours the tail is really separated from the coma by a broad dim gap. This gap broadens as the old tail moves with an accelerated motion downstream, and the new tail is build up much slower.

10. A corotating interaction region

The transition from slow to fast speed is not discontinuous. The fast and slow flows interact on their travel through the interplanetary space. What is observed at 1AU distance from the sun is described by Gosling et al. (1978). The behaviour of density, flow speed, flow angle and proton temperature across the interaction region is shown in Fig. 22 which is adapted from Fig. 1 of Gosling et al. (1978).

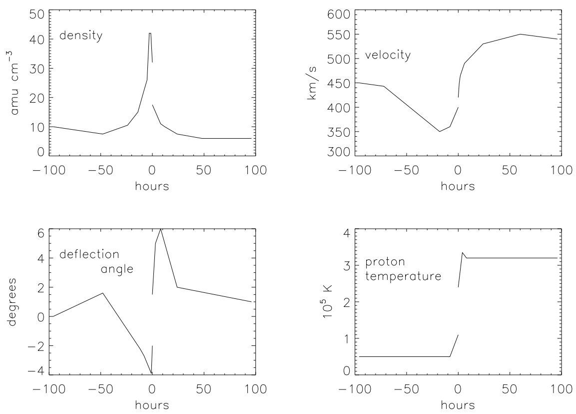

Fig. 22. Density, flow speed, flow angle and proton temperature across a CIR (adapted from Fig. 1 of Gosling et al. 1978). Abscissa = time in hours.

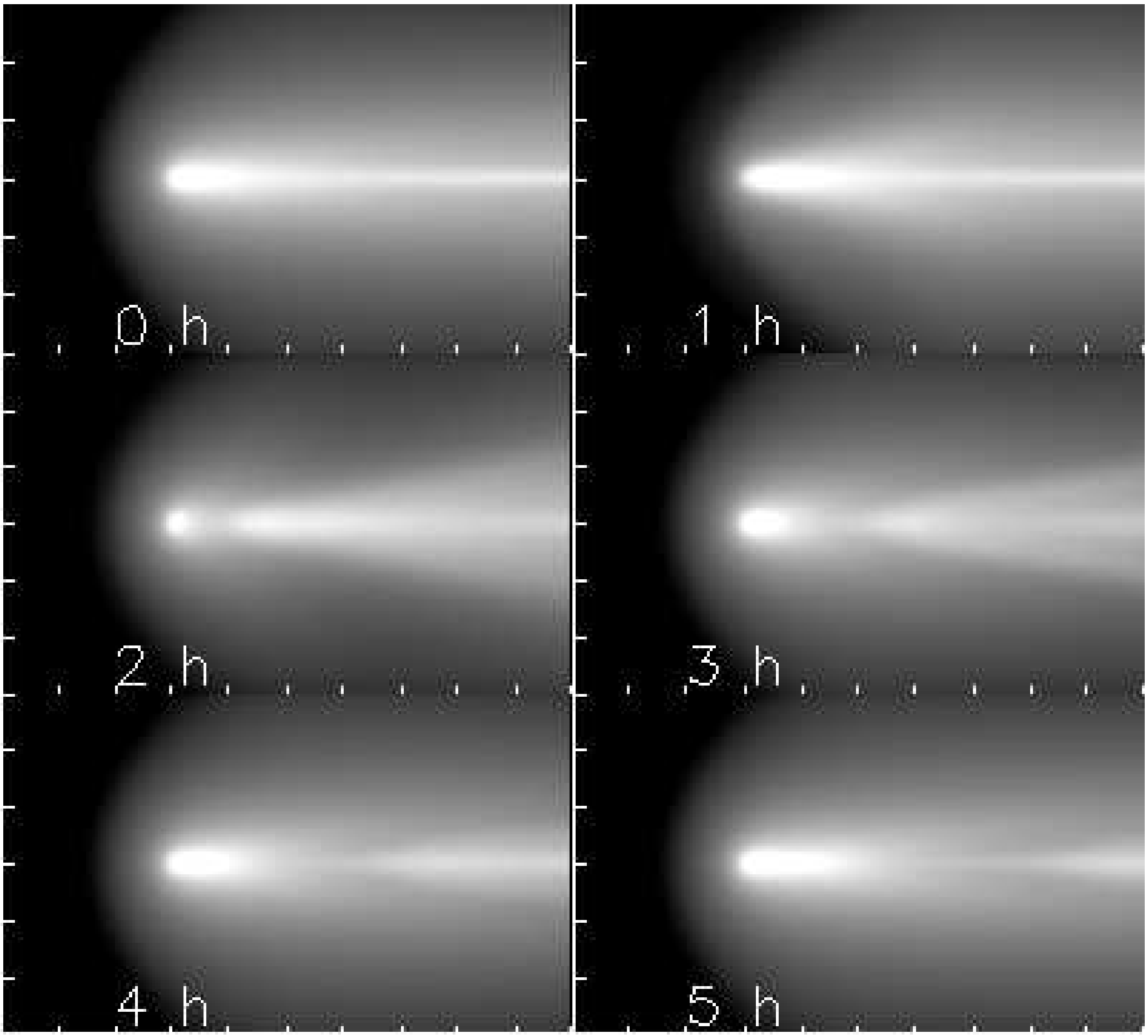

Fig. 18. The same as Figure 16 but in a projection onto the perpendicular plane.

The physical parameters change discontinuously at the stream interface. But they change already 1 - 2 days before, and continue to change after the interface. These changes on timescales of days should make most interesting effects on the tail of a big Halley type comet. We started a time-dependent calculation from the model 'big1' and varied the solar wind conditions as a function of time as shown in Figure 22. This is complemented by a magnetic field which is constant $B = 12$ nT for $t > 0$ and $B = 6$ nT for $t < -8$h, and increases linearly with time in the interval $-8 \leq t \leq 0$ according to Fig. 3 of Gosling et al. 1978. Time t=0 marks the instant when the interface first enters the computational grid. The computational region covers 1.56 $\times 10^6$ km in front and on the sides of the nucleus and 3.5 $\times 10^6$ km in the tail.

The most dramatic changes in the tail occur in the hours after the passage of the interface. Figure 23 shows that after 12h the tail has the signature of an HSS interaction as described in section 3. There is a kink in the tail where the tail appears to be torn apart. Figure 24 shows in its lower panel this kink at a distance of nearly 3 $\times 10^6$ km. The middle panel shows that the coma dims, and that a pronounced second brightness maximum in the tail develops. The upper panel demonstrates, that a substantial part of the ions is detached from the coma and moves downward. The tail becomes disconnected about 5.5h before the interface enters the grid. It starts from a position 120 000 km behind the nucleus and is accelerated with $a = 2$ m s^{-2}.

11. Observations

High speed streams have been caught 'with smoking gun' several times.

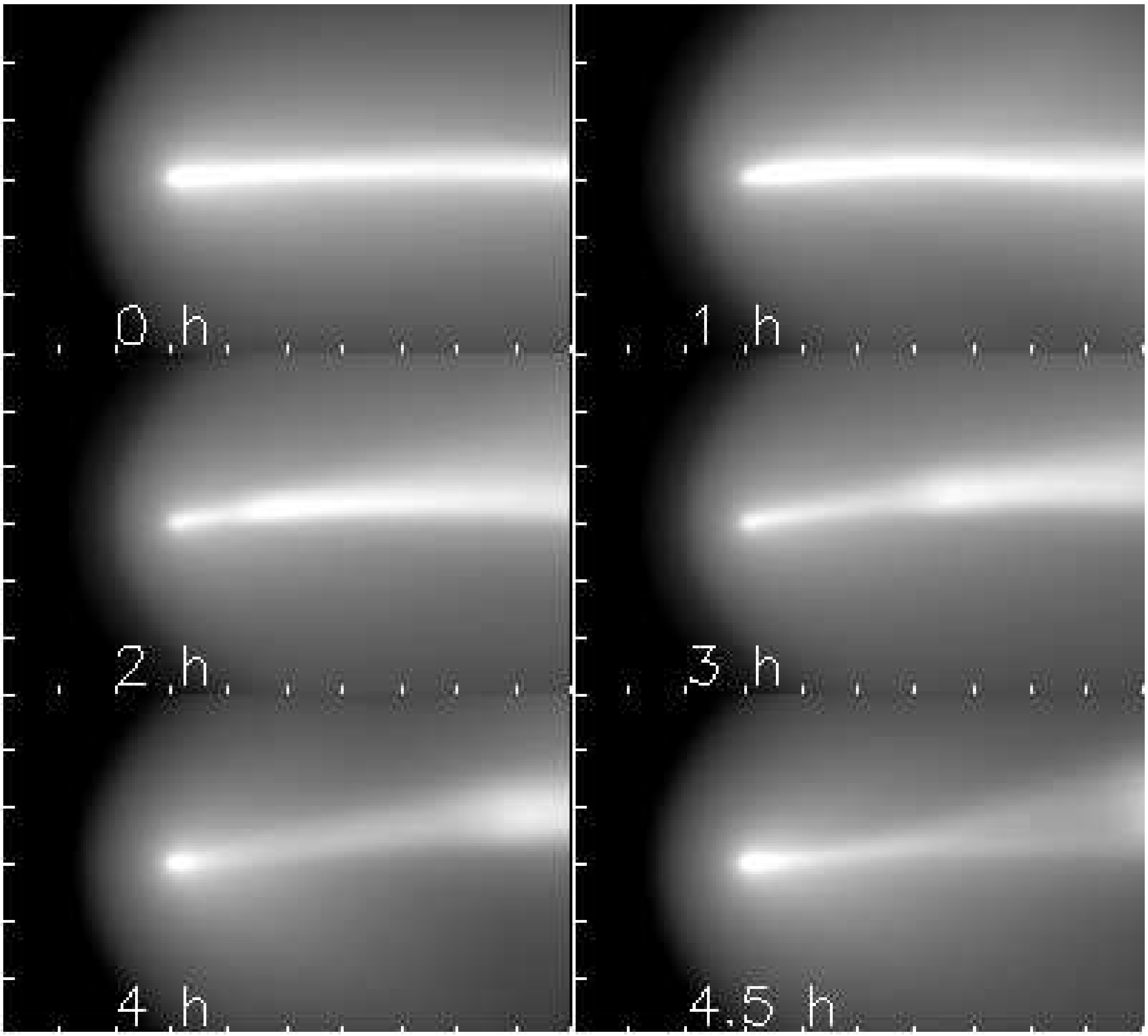

Fig. 19. The same as Figure 2 for an interplanetary shock of Mach 2. The last image is after 4.5 h.

Niedner et al. (1978) found an association between an event in comet Kohoutek's tail and a corotating HSS. A beautiful image of the comet on Jan 20 1974 is reproduced by Niedner et al. (1978) on plate 18. A schematic drawing of the tail (Niedner et al. 1978,Fig.4) at this date shows two nearly straight segments connected by a 'joint'. "The results [of Niedner et al. 1978] indicate that, at the time of formation of the perturbed tail structure, the comet was entering the compression region of [a] strong high-speed solar-wind ..." (Niedner et al. 1978,p.1014). This is elaborated further by Jockers (1981, 1985).

Later Niedner and Brandt (1978) noticed that also the HCS was close to the comet at the right time to trigger this event. Comparison of the two papers of Niedner and coworkers (1978) demonstrates that the association of cometary and solar wind events is not always unambiguous.

Jockers and Lüst (1973),p.116, interprete a kink in the tail of comet Bennett on April 6 1970 as being caused by the April 5 Solar Wind HSS. They also describe the three regions: The far tail has not yet noticed the fast wind, the near tail is in the new direction, the transition region connects both.

Brandt et al. (1980) investigate the rapid turning of the tail of comet Bradfield on 1980 February 6. They consider as cause a rapid change in velocity direction and note that "the likely location of these sharp gradients in flow are the leading edges of HSS ... and interplanetary shock fronts ..." (p. L54).

The collections of images (C88) of comet Halley's 1986 apparition made by Celnik et al. (1988), and the International Halley Watch Atlas (IHW) compiled by Brandt et al. (1992) provide us with ample material to study the morphology of a cometary plasma tail. Some prominent examples will be discussed here.

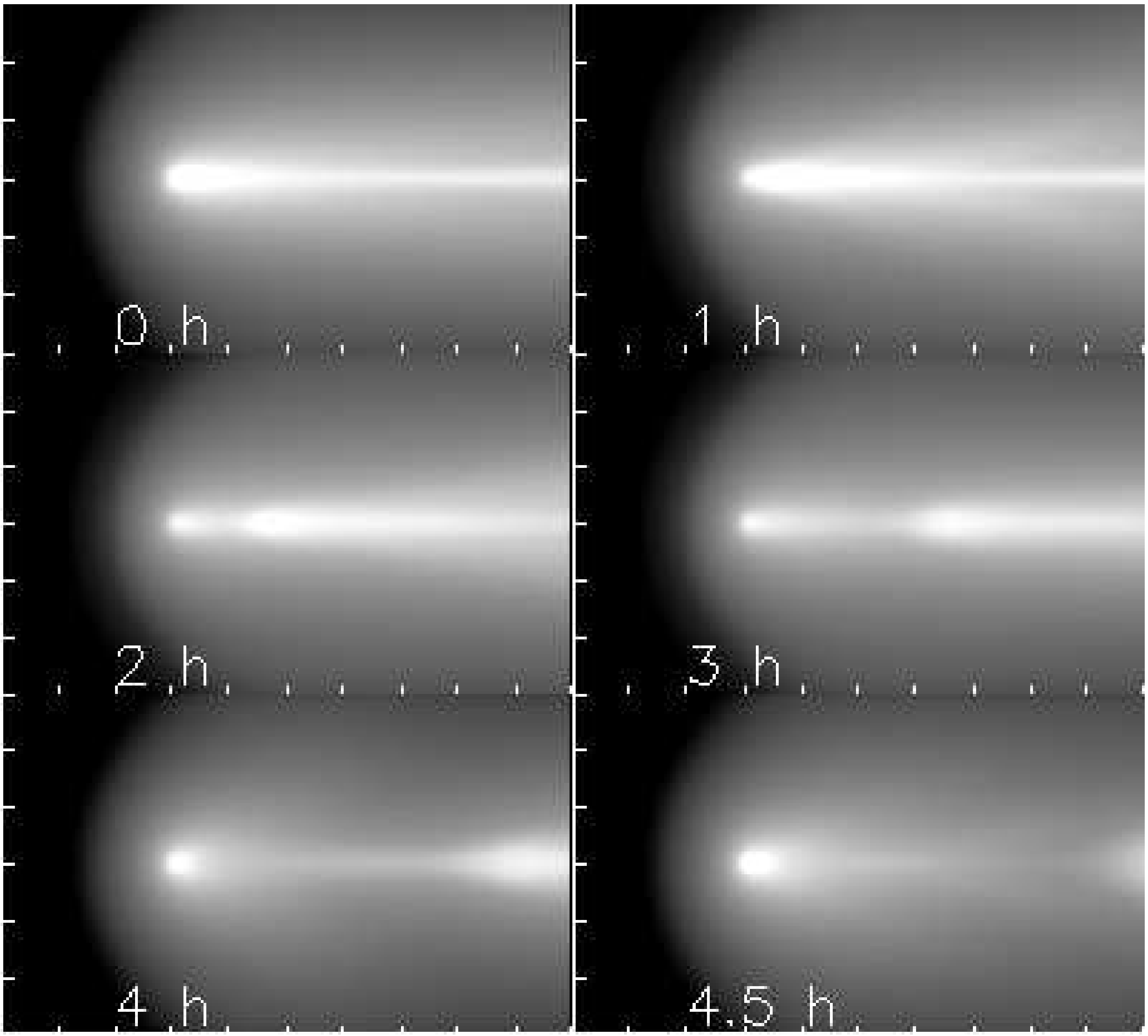

Fig. 21. The same as Figure 19 but in a projection onto the perpendicular plane.

March 9: Image 4993 in C88, and p. 195 of IHW show a well developed kink in the tail. We suspect an HSS as cause.

March 10: On image 5028 in C88, and on p. 198 of IHW the tail looks diagonally split. This event is discussed by Wu & Qiu (1987), where it is associated with a shock wave generated by a solar flare on March 6 at 16:37 UT. This fits very well to our model calculations (Wegmann 1995, see also Figure 19).

March 17: Image 5168 in C88 and p. 249 of IHW give another nice example of a kink.

March 20: On image 5241 in C88, and on p. 287 of IHW one can see a tail which is narrow close behind the nucleus but fans widely out at a position far behind the nucleus. This looks similar to what we obtained in our model calculations for the effect of an NCDE (see Figs. 16 and 18). On March 18 the spacecraft Sakigake, at that time still close to comet Halley, measured a solar wind density of about 40 cm^{-3}, the highest value in the five months interval reported by Oyama et al (1986). This lends some support to our interpretation that this event was generated by enhanced solar wind density. The front edge of the disconnected tail moved from 2.43 to 6.46 $\times$ 10^6 km distance with the nearly constant velocity of 37.0 – 40.4 km/s (Brosius et al. 1987, Table 3). This fits very nicely to the model results of section 8 where we found that the tail structure triggered by an NCDE travels finally with constant velocity. According to Celnik et al.(1988),p. 106, the position of the plasma tail structure,labeled p_2, at three consecutive nights March 21.33, 22.31, and 23.29 was 5.73, 12.19, and 19.4 $\times 10^6$ km behind the nucleus. This means that the structure moved after an intermediate acceleration again with a nearly constant velocity of 76 - 85 km s^{-1}.

April 8-9: Image 5771 in C88, and p. 377 of IHW provide an example of an event where apparently the whole

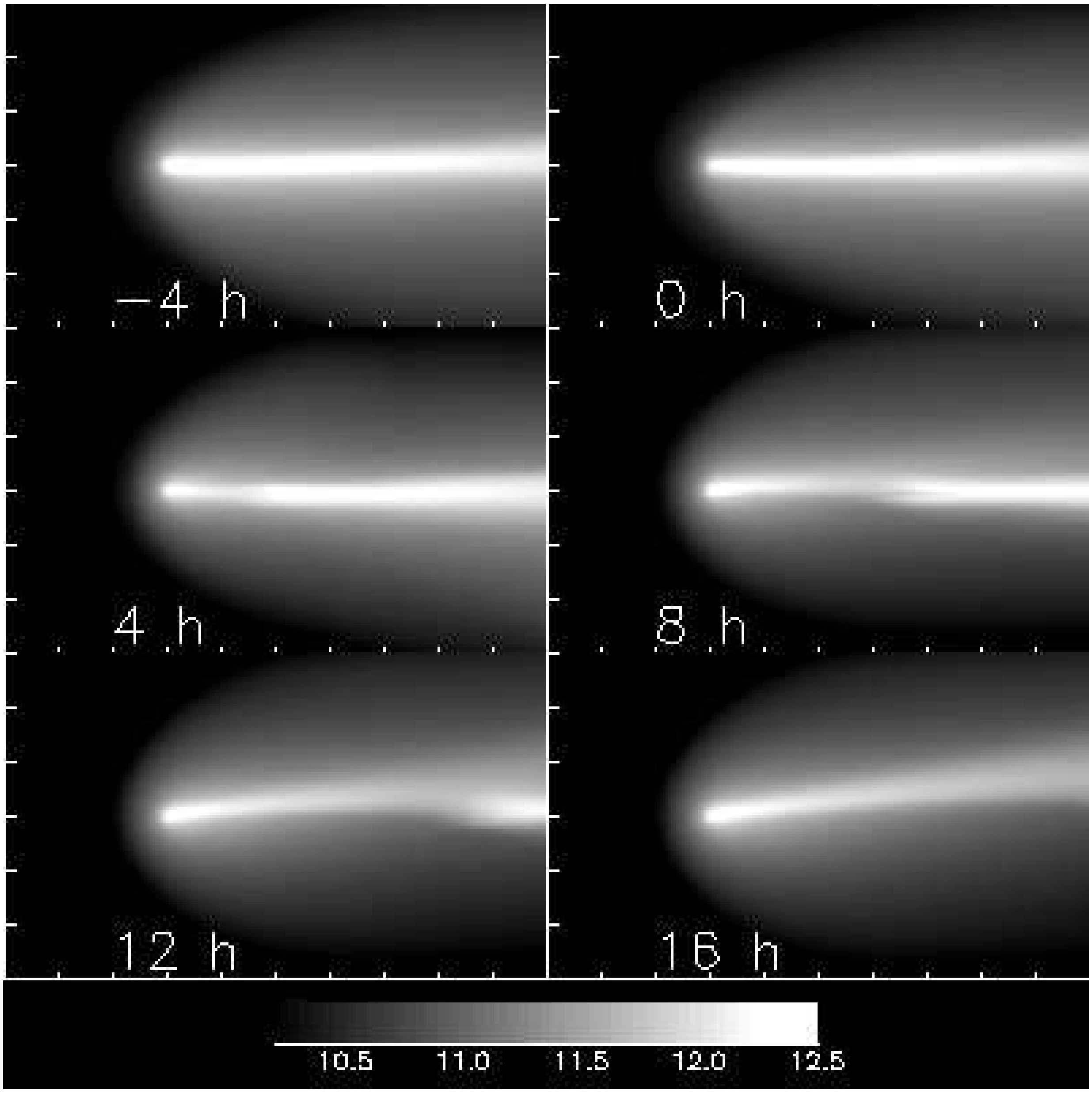

Fig. 23. Logarithms of the column densities [cm^{-2}] in a projection to the IMF plane -4,0,4,8,12,16 hours after a stream interface has entered at the lower left corner. The length scale is 500 000 km

tail is severed. The tail looks similar to what we see in our model calculation for the action of an interplanetary shock when the event is observed parallel to the IMF plane (see Figure 21).

April 11 -12: This event shown in Fig.2e of Brosius et al. (1987), and on page 429 in IHW can be correlated with solar wind data obtained by the ICE spacecraft. These data show in the 'arrival window' a magnetic field reversal accompanied with a density enhancement of more than a factor of 2 (Brosius et al. 1987, Fig.4). The tail on the image on page 429 in IHW looks like a cone with apex far behind the nucleus. The front edge of the disconnected tail moved from 1.08 to 4.12×10^6 km distance with the nearly constant velocity of 42.7 – 54 km/s (Brosius et al. 1987, Table 3). This phenomenology resembles closely to what our model calculations predict for the effect of an NCDE. We see here a current sheet in action, but it acts not via reconnection but via the associated density enhancement.

12. A dictionary

Rauer et al. (1995) calculated the effects of 1.) a change in solar wind flow, 2.) the rotation of the magnetic field by 90°, and 3.) a combination of velocity and magnetic field changes. They compared the model results with observations made by Bonev & Jockers (1994) at comet Austin

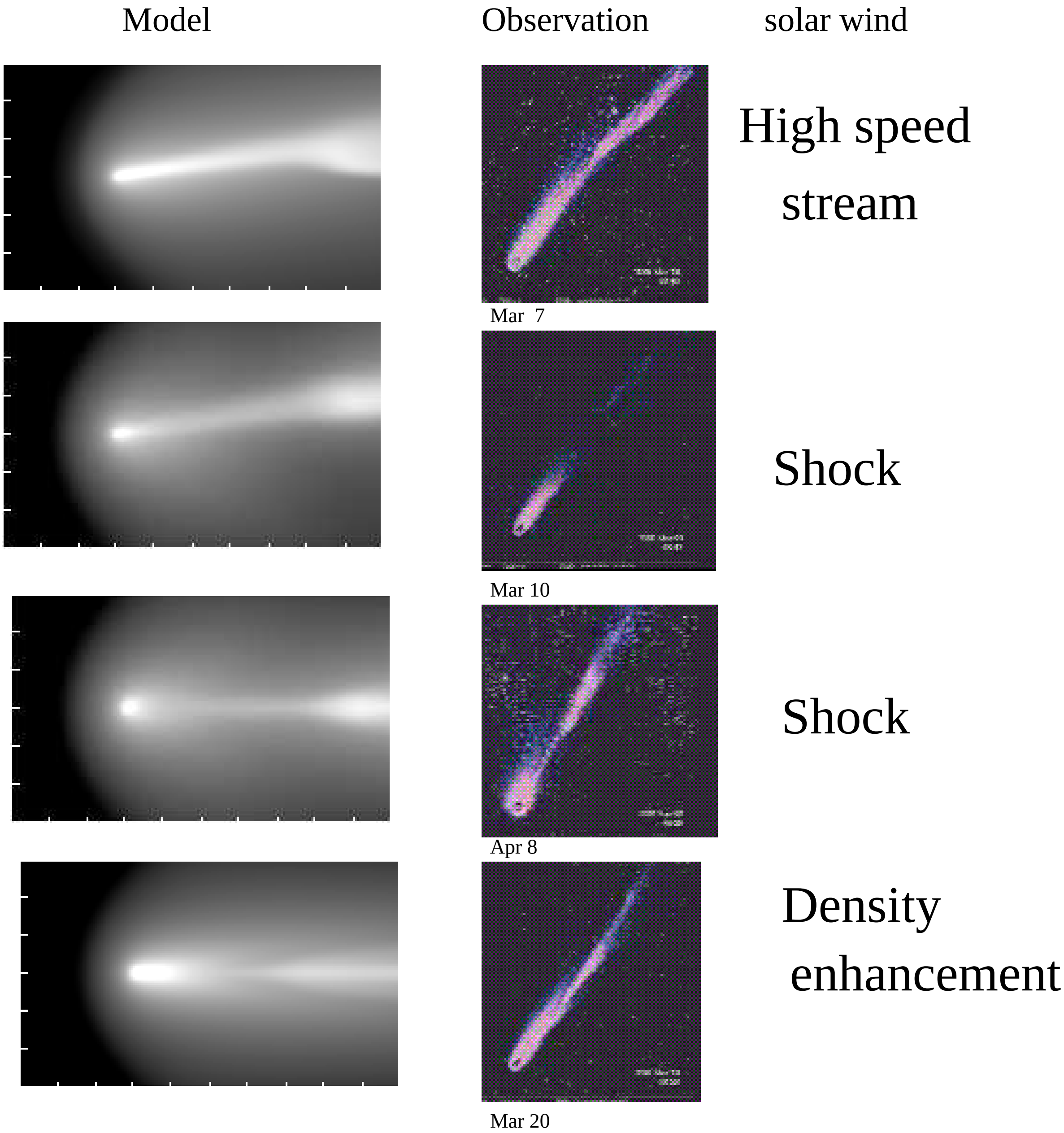

Fig. 25. An atlas of cometary tail morphologies: models (left column), observations (middle column) and their solar wind causes (right). The images of comet Halley 1986 are taken from a movie published by ESO in the internet.

1990 V. They summarized their results in a catalogue with entries of possible changes in the solar wind condition on one side and their effects on the cometary tail on the other side (Rauer et al. 1995, Table 3).

We can now summarize the results of our calculations in a similar way in a sort of dictionary which translates cometary events into solar wind causes. This translation is mediated by the connection between solar wind disturbances and cometary events found in our model calculations. The result is shown in Fig. 25. The left column shows the cometary tail found in the models four hours after the solar wind disturbance entered the computational grid. The right column denotes the triggering solar wind discontinuity. The middle column shows images of comet Halley's tail taken by ESO in 1986 and published as a movie in the internet. These rather coarse images show the essential features of the tail most clearly. They are therefore most suitable for comparison with our model results which admittedly are obtained on a rather coarse grid.

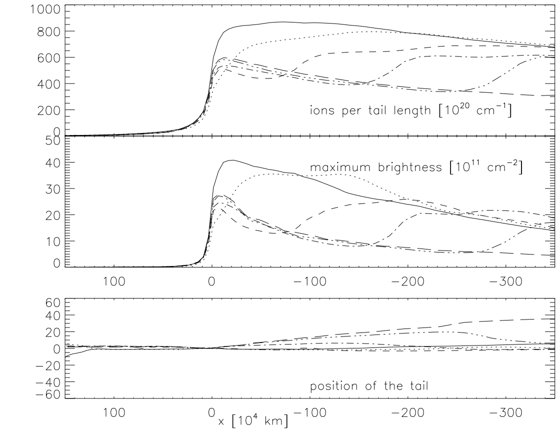

Fig. 24. The same as Figure 3 for a CIR.

13. Summary and conclusions

There are various disturbances in the solar wind. It is reasonable to expect that each of these has an effect on the plasma tail of comet which has its individual unique signature. We have performed MHD model calculations for several such solar wind disturbances, namely a high speed stream, a rotation of the flow velocity, a high speed stream without field enhancement, a sudden transition from fast to slow wind, a current sheet, a non compressive density enhancement, an interplanetary shock, and a corotating interaction region. It turns out that a HSS, a shock and an NCDE can trigger a tail disconnection. After an HSS there is a conspicuous kink in the tail, after a shock the tail looks diagonally split, and after a NCDE a broadly fanned out tail recedes with constant velocity. These features can be distinguished in observed DEs. There are some associations of observed DEs and observed solar wind disturbances, which confirm the results of our model calculations.

Movies showing the tail of a comet under the action of an HSS, an NCDE, or a shock can be obtained under the internet address:

`http://www.mpa-garching.mpg.de/~ruw/comets`

References

Bonev T., Jockers K., H_2O^+ ions in the inner plasma tail of comet Austin 1990 V, *Icarus* **107**, 335–357 1994

Brandt J.C., Hawley J.D., Niedner Jr. M.B., A very rapid turning of the plasma-tail axis of comet Bradfield 1979l on 1980 February 6, *Astrophys. J.*, **241** , L51–L54, 1980

Brandt J.C., Observations and dynamics of plasma tails, in *Comets*, ed. L.L.Wilkening, Univ. of Arizona Press, 519–537, 1982

Brandt J.C., Niedner Jr. M.B., Rahe J., *The International Halley Watch Atlas of Large-Scale Phenomena,* University of Colorado-Boulder, 1992

Brandt J.C., Caputo F.M., Hoeksema J.T., Niedner Jr.M.B., Yi Y., Snow M., Disconnection events (DEs) in Halley's comet 1985-1986: The correlation with crossings of the heliospheric current sheet (HCS), *Icarus* **137** , 69–83, 1999

Brosius J.W., Holman G.D., Niedner M.B., Brandt J.C., Slavin J.A., Smith E.J., Zwickl R.D., Bame S.J., The cause of two plasma-tail disconnection events during the ICE-Halley radial period, *Astron.& Astrophys.* **187** ,267–275, 1987

Celnik W.E., Schmidt-Kaler Th., Structure and dynamics of plasma-tail condensations of comet P/Halley 1986 and inferences on the structure and activity of cometary nucleus, *Astron. Astrophys.* **187**, 233–248, 1987

Celnik W.E., Koczet P., Schlosser W., Schulz R., Svejda P., Weißbauer K., Structure and dynamics of plasma tail condensations of comet P/Halley 1986, *Astron. Astrophys. Suppl.* **72**, 89–127, 1988

Delva M., Schwingenschuh K., Niedner M.B., Gringauz K.I., Comet Halley remote plasma tail observations and *in situ* solar wind properties: *VEGA*-1/2 IMF/Plasma observations and ground-based optical observations from 1 December 1985 to 1 May 1986, *Planet.Space Sci.* **39**, 697–708, 1991

Farnham T.L, Meech K.J., Comparison of the plasma tails of four comets: P/Halley, Okazaki-Levy-Rudenko, Austin, and Levy, *Astrophys. J. Suppl.*, **91**, 419 – 460,1994

Fedder J.A., Brecht S.H., Lyon J.G., MHD simulation of a comet magnetosphere, *Memo. Rep. 5306,* Nav. Res. Lab., Washington, D.C., 1984

Gombosi T.I., Powell K.G., de Zeeuw D.L., Axisymmetric modeling of cometary mass loading on an adaptively refined grid: MHD results, *J.Geophys.Res.* **99**, 21 525–21 539, 1994

Gosling J.T., Hildner E., Asbridge J.R., Bame S.J., Feldman W.C., Noncompressive density enhancements in the solar wind, *J.Geophys.Res.* **82**, 5005–5010, 1977

Gosling J.T., Asbridge J.R., Bame S.J., Feldman W.C., Solar wind stream interfaces, *J.Geophys.Res.* **83**, 1401–1412,1978

Gosling J.T., Borrini G., Asbridge J.R., Bame S.J., Feldman W.C., Hansen R.T., Coronal streamers in the solar wind at 1 AU, *J.Geophys.Res.* **86**,5438–5448, 1981

Jockers K., Lüst Rh., Tail peculiarities in comet Bennett caused by solar wind disturbances, *Astron. & Astrophys.* **26**, 113–121, 1973

Jockers K., Plasma dynamics in the tail of comet Kohoutek 1973 XII, *Icarus* **47**, 397 –411, 1981

Jockers K., The ion tail of comet Kohoutek 1973 XII during 17 days of solar wind gusts, *Astron, Astrophys. Suppl.* **62**,791–838, 1985

Niedner M.B.Jr., Rothe E.D., Brandt J.C., Interplanetary gas XXII. Interaction of comet Kohoutek's ion tail with the compression region of a solar-wind corotating stream, *Astrophys. J.* **221**, 1014–1025, 1978

Niedner M.B.Jr. , Brandt J.C., Interplanetary gas XXIII. Plasma tail disconnection events in comets: Evidence for magnetic field line reconnection at interplanetary sector boundaries? *Astrophys. J.* **223**, 655–670, 1978

Niedner M.B.Jr., Dynamics of cometary plasma tails, *Adv. Space Res.* **6**,315–327, 1986

Oyama K., Hirao K., Hirano T., Yumoto K., Saito T., Was the solar wind decelerated by comet Halley? *Nature* **321**, 310–313, 1986

Rauer H., Wegmann R., Schmidt H.U., Jockers K., 3-D MHD simulations of the effect of comoving discontinuities in the solar wind on cometary plasma tails, *Astron. Astrophys.* **295**, 529–550, 1995

Schmidt H.U., Wegmann R., Plasma flow and magnetic fields in comets, in *Comets*, ed. L.L.Wilkening, Univ. of Arizona Press, 538–560, 1982

Schmidt-Voigt M., Time-dependent MHD simulations for cometary plasmas, *Astron & Astrophys.* **210**, 433–454, 1989

Slavin J.A., Goldberg B.A., Smith E.J., McComas D.J., Bame S.J., Strauss M.A., Spinrad H., The structure of cometary type I tail: Ground-based and ICE observations of P/Giacobini-Zinner, *Geophys. Res. Letts.* **13**, 1085–1088, 1986

Voelzke M.R., Matsuura O.T., Morphological analysis of the plasma structures of comet P/Halley, *Planet.Space Sci.* **46**, 835–841, 1998

Wegmann R., MHD model calculations for the effect of interplanetary shocks on the plasma tail of a comet, *Astron & Astrophys.* **294**, 601 – 614, 1995

Wegmann R., Schmidt H.U., Bonev T., The three-dimensional structure of the plasma tail of comet Austin 1990 V, *Astron & Astrophys.* **306**, 638–644, 1996

Wegmann R., Jockers K., Bonev T., H_2O^+ ions in comets: Models and observations, *Planet. Space Sci.* **47**, 745–763, 1999

Wegmann R., Schmidt H.U., Dennerl K., Englhauser J., Analysis of the X-ray emission of comets, in preparation

Winterhalter D., Smith E.J., Burton M.E., Murphy N., McComas D.J., The heliospheric plasma sheet, *J.Geophys.Res.* **99**, 6667–6680, 1994

Wu M.C., Qiu P.Z., Activity of the plasma tail of comet P/Halley in March, 1986, *Astron & Astrophys.* **187**, 264–266, 1987

Yi Y., Caputo F.M., Brandt J.C., Disconnection events and sector boundaries: The evidence from comet Halley 1985-1986, *Planet.Space Sci.* **42**, 705–720, 1994

Yi Y., Walker R.J., Ogino T., Brandt J.C., Global magnetohydrodynamic simulation of a comet crossing the heliospheric current sheet, *J.Geophys.Res.* **101**, 27 585 –27 601, 1996